Monthly Notices
of the
ROYAL ASTRONOMICAL SOCIETY

MNRAS **429,** 429–443 (2013) doi:10.1093/mnras/sts346

Extended and filamentary Lyα emission from the formation of a protogalactic halo at $z = 2.63$⋆†

Michael Rauch,[1‡] George D. Becker,[2] Martin G. Haehnelt,[2,3] Jean-Rene Gauthier[4] and Wallace L. W. Sargent[4]

[1]*Carnegie Observatories, 813 Santa Barbara Street, Pasadena, CA 91101, USA*
[2]*Institute of Astronomy and Kavli Institute for Cosmology, Cambridge University, Madingley Road, Cambridge CB3 0HA*
[3]*Kavli Institute for Theoretical Physics, Kohn Hall, University of California, Santa Barbara, CA 93106-4030, USA*
[4]*Palomar Observatory, California Institute of Technology, Pasadena, CA 91125, USA*

Accepted 2012 November 1. Received 2012 October 26; in original form 2012 June 12

ABSTRACT

We report the observation of a further asymmetric, extended Lyα emitting halo at $z = 2.63$, from our ultra-deep, long-slit spectroscopic survey of faint high-redshift emitters, undertaken with Magellan LDSS3 in the GOODS-S field. The Lyα emission, detected over more than 30 kpc, is spatially coincident with a statistically significant concentration of galaxies visible in deep broad-band imaging. While these faint galaxies without spectroscopic redshifts cannot all with certainty be associated with one another or with the Lyα emission, there are a number of compelling reasons why they very probably form a Milky Way halo-mass group at the Lyα redshift. Filamentary structure, possibly consisting of Lyα emission with very high equivalent width, blue stellar continua and evidence for disturbed stellar populations, suggest that the properties of the emitting region reflect ongoing galaxy assembly, with recent galaxy mergers and star formation occurring in the group. The Lyα emission may be powered by cooling radiation or spatially extended star formation in the halo, but is unlikely to be fluorescence driven by either an active galactic nucleus or one of the galaxies. A comparison with the Lyα surface brightness profiles of more typical, bright Lyα emitters or Lyman break galaxies from similarly deep two-dimensional spectra shows them to be conspicuously different from the extended, asymmetric object studied here. This is consistent with the picture that typical Lyα emitters represent Lyα resonantly scattering from single, kinematically quiescent, compact sources of ionizing radiation, whereas extended emission of the kind seen in the current halo reflect a more active, kinematically disturbed stage in the galaxy formation process. Hence, unusual Lyα emission as observed here may provide unique insights into what is probably a key mode of galaxy formation at high redshifts. Our observations provide further, circumstantial evidence that galaxy mergers may promote the production and/or escape of ionizing radiation, and that the haloes of interacting galaxies may be significant sources for ionizing photons during the epoch of reionization.

Key words: galaxies: dwarf – galaxies: evolution – galaxies: interactions – intergalactic medium – dark ages, reionization, first stars – diffuse radiation.

1 INTRODUCTION

Present-day galaxies are thought to have grown through a combination of mergers and the continued accretion of gas from the intergalactic medium (IGM). Theoretically, this picture is well motivated (White & Rees 1978), but considerable uncertainties remain about the relative roles of mergers, the inflow of fresh and recycled gas, and the expulsion of gas due to stellar and active galactic nucleus (AGN) feedback and through interactions.

⋆This paper includes data gathered with the 6.5-m Magellan Telescopes located at Las Campanas Observatory, Chile.
† Some of the data presented herein were obtained at the W. M. Keck Observatory, which is operated as a scientific partnership among the California Institute of Technology, the University of California and the National Aeronautics and Space Administration. The Observatory was made possible by the generous financial support of the W. M. Keck Foundation.
‡ E-mail: mr@obs.carnegiescience.edu

Observational studies of the *emission* from high-redshift galaxies have mostly concerned themselves with the compact stellar populations of galaxies, whereas narrow-band and spectroscopic studies aiming at the gaseous component have been restricted to the bright end of the luminosity function and the progenitors of the most massive present-day galaxies. Studies of the much less massive building blocks of more typical low-z objects until very recently had to rely on observations of intervening absorption line systems in the spectra of high-redshift background QSOs.

At redshift $\sim$3, a future Milky Way like galaxy is expected to consist of a group of mostly faint protogalaxies, spread out over a region spanning several hundred kpc (proper). QSO metal absorption systems and damped Lyα systems (DLAS) have provided insights into the gaseous environment of these newly forming galactic haloes. A picture of multiple, gaseous protogalactic clumps, accreting gas and ultimately merging, has been used to successfully model the properties of observed QSO absorption systems (e.g. Haehnelt, Steinmetz & Rauch 1996; Rauch, Haehnelt & Steinmetz 1997). Theoretical modelling has also shed light on the likely geometry of the gas accretion process and the relative importance of the various accretion modes (e.g. Birnboim & Dekel 2003; Kereš et al. 2005; Dekel & Birnboim 2006; Dekel et al. 2009; Fumagalli et al. 2011a; van de Voort et al. 2011).

Ultra-deep spectroscopic surveys (e.g. Bunker, Marleau & Graham 1998; Santos et al. 2004; Rauch et al. 2008, 2011) have reached surface brightness limits where it becomes possible to trace the progenitors of present-day galaxies and some of their protogalactic building blocks directly in Lyα emission, at radii out to tens of kpc. The deep spectroscopic FORS–VLT survey by Rauch et al. (2008; see also Barnes & Haehnelt 2010; Rauch & Haehnelt 2011) appears to have detected the bulk of the host galaxies of DLAS and Lyman limit systems (LLS) at $z \sim 3$ in the form of faint Lyα emitting galaxies, with space densities reaching $3 \times 10^{-2}\ h_{70}^3$ Mpc^{-3}. Clustering studies of the generally brighter Lyα emitters found by narrow-band imaging surveys suggest that these studies are probing the massive end of the same progenitor population (e.g. Guaita et al. 2010).

The progenitors of present-day galaxies are expected to undergo repeated mergers. Interactions of the merging constituents with the ambient halo medium and among each other may transform the properties of the stellar populations and the physical state of the gas in ways observable even at high redshift. For example, intriguing evidence for the connection between Lyα emission and the small-scale galactic environment has been presented by Cooke et al. (2010), who found spatially close pairs of Lyman break galaxies to show a very high fraction of Lyα emitters. The Lyα photons may be escaping because of damage to the optically thick gaseous halo during encounters (e.g. Hibbard, Vacca & Yun 2000), or may result from star formation, perhaps induced in the halo by tidal tails or ram-pressure-stripped gas, or by nuclear inflows. These effects may also work to increase the production and favour the release of ionizing radiation, turning mergers into promising sites for the sources of ionizing photons during the epoch of reionization (e.g. Bridge et al. 2010; Rauch et al. 2011, hereafter Paper I).

Immediate observational signatures of Lyα emitters caused by interactions may include spatially extended Lyα emission, a disturbed velocity field imprinted on the Lyα emission line and the presence of multiple sources of continuum and ionizing radiation. These characteristics suggest that these objects are best approached by a combination of deep spectroscopy (for the detection and velocity structure of the gaseous haloes) with deep space-based imaging (to study the stellar populations and the geometry).

Two such surveys have now been performed by us in the Hubble Deep Field North (HDFN, with Keck I/LRIS) and the Hubble Deep Field South (HUDF, with Magellan/LDSS3), and the respective GOODS flanking fields, taking advantage of existing space-based imaging. Among the generally compact Lyα emitters, a small fraction are found that show pronounced spatial asymmetries relative to a continuum source and extended morphologies (diameters of several arcseconds, to the detection levels reached) in Lyα emission. With a space density of $\sim 10^{-3}\ h_{70}^3$ Mpc^{-3} (where h_{70} is the Hubble constant in units of 70 km s^{-1} Mpc^{-1}) and fluxes of a few times 10^{-17} erg cm^{-2} s^{-1}, these objects are more common and fainter than the so-called 'Lyα blobs' (e.g. Francis et al. 1996; Fynbo, Møller & Warren 1999; Keel et al. 1999; Steidel et al. 2000; Palunas et al. 2004; Matsuda et al. 2004, 2011, 2012; Dey et al. 2005; Nilsson et al. 2006; Ouchi et al. 2009; Prescott et al. 2009, 2012; Scarlata et al. 2009; Yang et al. 2009, 2010, 2011; Bridge et al. 2012), although, as we shall discuss below, they share some similarities.

Of the three brightest objects matching these criteria in the HUDF, the first one is the interacting $V \sim 27$, $z = 3.34$ object described in Paper I, the second is the object to be described here and the remaining one (to be published) turned out to be the optical counterpart of an obscured X-ray bright $z = 3$ QSO.

This paper is organized as follows. The observations of the $z = 2.63$ Lyα halo are presented, starting with an analysis of the spectroscopic properties of the Lyα emission line region. We then examine *Hubble Space Telescope* (*HST*)/ACS images for clues about the underlying stellar populations. The detection of a filamentary structure likely to be glowing in Lyα is described in the next section, followed by a discussion of possible origins of the radiation. The nature of the underlying association of objects is examined in the context of dark matter haloes, concluding with a comparison between the extended emitters discussed here and the more common 'compact' Lyα emitters and Lyα emitting Lyman break galaxies. Simple models for the surface brightness distribution of the compact emitters are used to obtain insights into the nature of the underlying gaseous halo. An appendix consisting of two sections describes how a lag between an instantaneous starburst and Lyα recombination radiation can maintain detectable Lyα emission and a high equivalent width beyond the decline of the stellar sources of ionizing radiation (Appendix A) and how the observations of the high signal-to-noise ratio surface brightness profiles of individual Lyα emitters from our surveys can constrain the line formation process (Appendix B).

2 OBSERVATIONS

The object described here was discovered in the long-slit, spectroscopic, blind survey in the Hubble Ultra Deep Field (HUDF)/GOODS-South field (Giavalisco et al. 2004; Beckwith et al. 2006) described in Paper I. The data are based on a spectrum taken with the LDSS3 spectrograph on the Magellan II telescope at Las Campanas. Using a 2 arcsec $\times$ 8.3 arcmin long slit at a position angle of 0° and the VPH blue grating, a set of 3000-s long exposures totalling 61.4 h of useful exposure time was recorded during 2008 November 18–23 and 2009 November 11–16. The spectra consist of 0.186-arcsec wide pixels, with a measured spatial full width at half-maximum (FWHM) of 0.85 arcsec in the spectral region of interest and a slit-width limited resolution of 340 km s^{-1} (FWHM). The useable survey volume was $2056\ h_{70}^{-1}$ Mpc^{-3} at a mean redshift of 3.33.

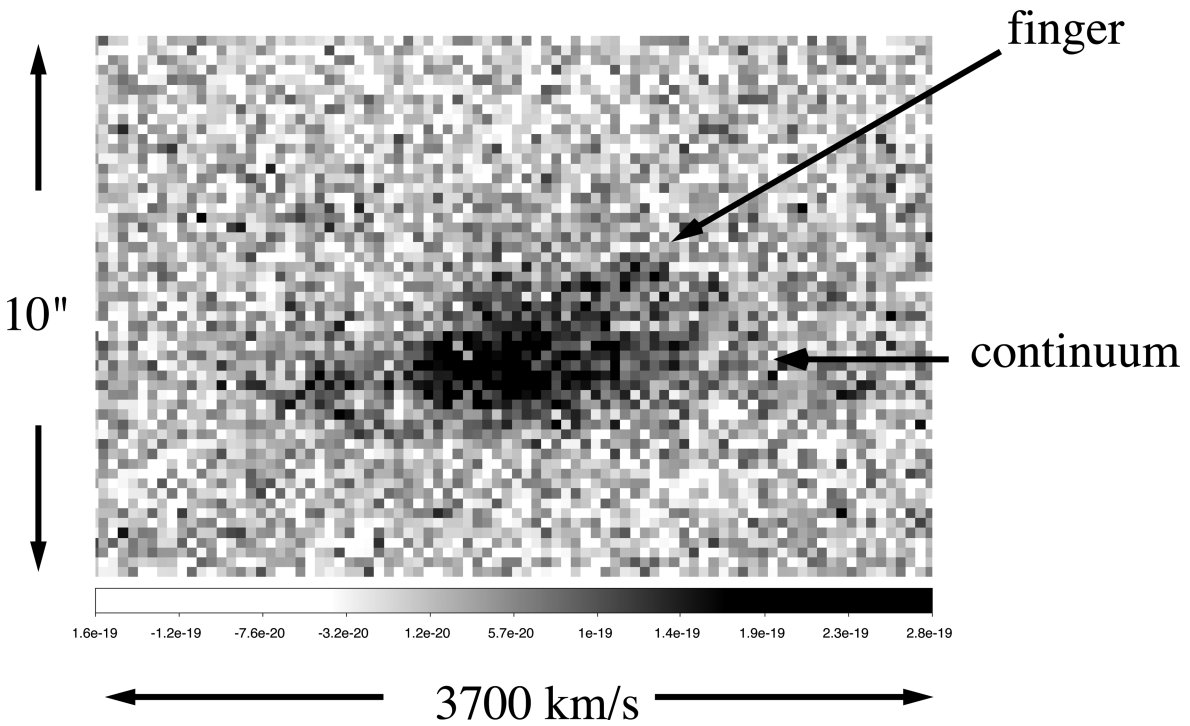

Figure 1. Spectrum of the $z = 2.63$ Lyα emission line. The wavelength increases towards the right. The vertical direction is the spatial coordinate along the slit, which was oriented at a position angle of 0°, i.e. north–south. The spatial extent along the slit of the section shown here is 10 arcsec and the velocity extent in the spectral (horizontal) direction is about 3700 km s^{-1}. The 1σ fluctuation in the flux density per 0.185 arcsec × 0.64 Å wide pixel is 5×10^{-20} erg cm^{-2} s^{-1} Å^{-1}. The arrows show the approximate horizontal position of the strongest continuum trace (caused by object A, see Fig. 2) and of a spatially extended Lyα 'finger'.

2.1 Spectroscopic data

The object is the second of three spatially extended, asymmetric (with respect to the brightest spectroscopically detectable continuum underlying the Lyα emission), relatively bright ($F > 2 \times 10^{-17}$ erg cm^{-2} s^{-1}) Lyα emitters in the survey. The Lyα line peaks at 4414.4 Å (Fig. 1), corresponding to redshift $z = 2.631$. The total line flux observed through the 2-arcsec wide slit amounts to $(3.7 \pm 0.2) \times 10^{-17}$ erg cm^{-2} s^{-1} (statistical errors only), which must be considered a lower limit, given the possibly considerable aperture losses. Similarly, the observed equivalent width, found to be 31.7 Å in the rest frame, from a comparison of the Lyα flux to the flux the brightest continuum traces immediately redward of the Lyα line, is a measure of limited usefulness because of its aperture dependence. The maximum spatial extent of the Lyα emission line in the vertical direction (i.e. north–south) along the slit is about 3.9 arcsec (32 kpc proper). In the spectral direction, the flux density is detectable at the $\sim 10^{-19}$ erg cm^{-2} s^{-1} Å^{-1} level over about 1800 km s^{-1}. The line consists of a clumpy, multi-humped profile with a dominant asymmetric red peak, showing an extended red shoulder. The width of the red peak if crudely fitted by a Gaussian profile is about 870 km s^{-1} at the location of the brightest continuum trace (see arrow in Fig. 1).

2.2 Broad-band detections of galactic counterparts

The position of the Lyα emitter along the slit coincides in projection with what appears to be a small group of galaxies within a few arcseconds of each other (Fig. 2, middle and right-hand panels). The position of a continuum trace (hard to see with the colour stretch applied here and indicated in Fig. 1 by a horizontal arrow) appears offset to the south from the peak of the extended emission. It is caused mainly by an object at 03:32:38.888 −27:44:29.07 we denote as 'A' in Fig. 2, with a fainter nearby object here called 'C'. The Lyα emission appears to stretch north (and redward) in a 'finger' of emission reaching somewhat beyond the declination of object 'B', suggesting that B may possibly belong to the same halo as A and so may C. The object 'D' is a foreground interloper. Its redshift can be identified in our spectrum from an [O II] 3728 Å doublet as $z = 0.663$. The centroids of the continuum traces of objects D and A are separated by 2.8 arcsec along the slit (i.e. in the north–south direction). The names in the literature for the objects and the various redshift measures are given in Table 1.

At least two other continuum sources occur within less than about 6 arcsec (48.8 kpc proper) of A, with similar $B - V$ colours, namely 'E' and 'F'. Moreover, two extended regions of emission with an appearance reminiscent of tidal features ('T1' and 'T2') are visible to the west and south-west of A, and a faint extended region T3 is seen just south of D and east of B. Both B and T3 in the image are lining up in projection with the narrow Lyα 'finger' extending to the upper right in the two-dimensional spectrum (e.g. Fig. 1). Below we shall argue that at least T3 may be linked causally to the Lyα 'finger'.

The faint region 'T1' extends about 1.3 arcsec to the south-west of object A and appears to be a continuum source, as it is visible in both B and V bands. This simultaneous detection strongly suggests the reality of the T1 feature, and its spatial connection to galaxy A suggests that it is indeed at the redshift of the halo. Additionally, in the B-band image, a thin filament of emission ('T2') extends 3.5 arcsec west from galaxy A, ending in another very faint object, 'F'. The latter is also visible simultaneously in B and V. Its projected connection with object F suggests that the structure T2

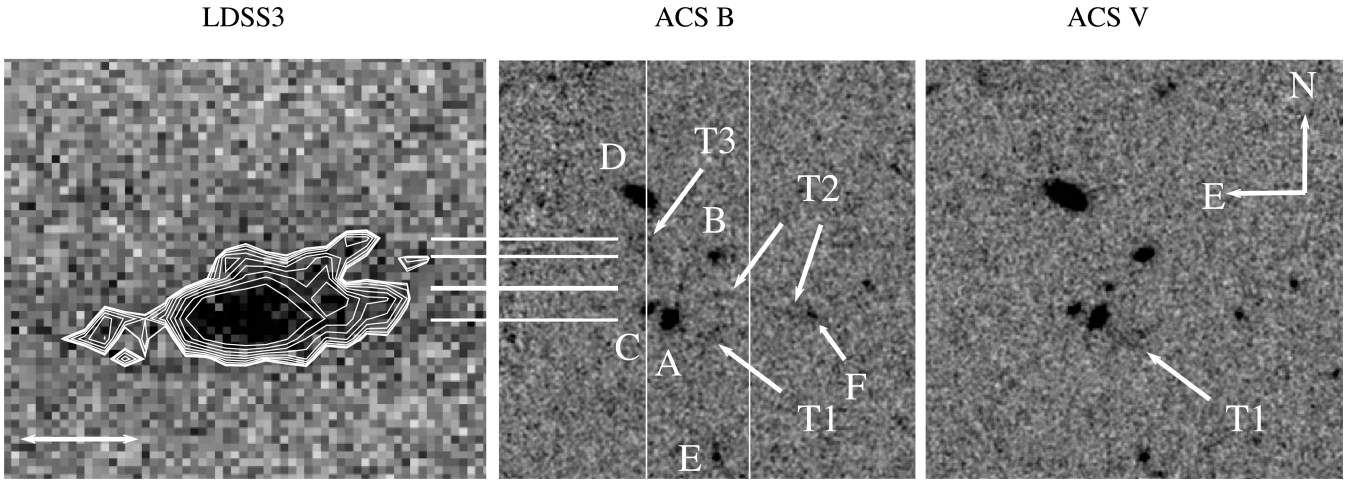

Figure 2. Lyα line spectrum and GOODS-S ACS imaging. Left-hand panel: the LDSS3 spectrum of the Lyα line at 4414 Å. For better visibility of the lower light level region, we have added white contours showing the Lyα emission flux density. The outermost contour corresponds approximately to 10^{-19} erg cm^{-2} s^{-1} Å^{-1}. The length of the white double arrow indicates a velocity scale of 600 km s^{-1}. Middle panel: 10 × 10 arcsec^2 *B*-band ACS image, centred on 03:32:38.821 −27:44:27.90 (2000). The two solid vertical lines denote the position of the slit edges, as determined by matching the flux profile in the slit direction with synthetic profiles obtained from projections of the ACS image. Object D is a $z = 0.663$ foreground object. Several of the other galaxies may be at the redshift of the Lyα halo. An extended stellar, possibly tidal patch of emission is indicated by the arrow marked with 'T1'. A thin filament of emission ('T2') appears to connect another faint compact object ('F') with what appears to be an even fainter one close to the centre of the field. A patchy spot of emission ('T3') can be discerned just south of the object D. The horizontal white lines indicate the positions along the slit in the south–north direction of the four one-dimensional spectra in Fig. 3. Right-hand panel: ACS *V*-band image. Note the persistence of feature T1 but not T2 or T3, as compared to the *B*-band image.

Table 1. GOODS-S objects.

ID	$z_{\rm spec}$	$z_{\rm phot}$	GOODS[a]	COMBO-17[b]/MUSIC[c]	$V\,(F606W)$[a]	$B-V$
A	2.631[d], 2.6191[e], 2.619[f]	1.91[b], 1.49[c], 2.066[f]	J033238.89−274429.1	40 596/13 597	25.12 ± 0.02[a]	0.20 ± 0.03[a]
B	2.631[d](?)	0.043[b], 3.06[c]	J033238.81−274427.6	40 626/13 635	26.06 ± 0.04[a]	1.01 ± 0.11[a]
C	2.631[d](?)	–	J033238.93−274428.9	–/–	27.33 ± 0.06[a]	0.25 ± 0.11[a]
D	0.663[d]	0.681[b], 0.69[c]	J033238.94−274426.2	40 690/13 640	24.46 ± 0.02[a]	0.76 ± 0.04[a]
E	?	2.092[f]	J033238.80−274432.4	–/–	27.92 ± 0.08[a]	0.34 ± 0.15[a]
F	?		J033238.63−274429.0	–/–	28.92 ± 0.18[a]	0.27 ± 0.32[a]
Filament T2	?	$2.2 < z < 2.9$[g]	–	–/–	>29.44	<-1.71[h]

[a]Giavalisco et al. (2004), from the h_goods_sv_r1.1z.cat.txt catalogue file; [b]Wolf et al. (2001); [c]Grazian et al. (2006); [d]this paper; [e]Balestra et al. (2010); [f]Cardamone et al. (2010); [g]from the wavelength limits of the *B*-band filter which would limit the redshift of the presumed Lyα emission to those values; [h]1σ, in custom aperture.

is real as well. The T2 structure, which we shall discuss further below, is invisible in the *V* band, as is T3. T2 and T3 are detected in the *B* band against the background noise at the 4.7σ and 7.9σ levels, respectively, as will be shown below. It is somewhat hard to judge the reality of these features from Fig. 2, especially given that the background noise level in the *B* band rises abruptly in part of the upper left-hand quadrant, but the interested reader may directly download the publicly available images from the STScI archive (http://archive.stsci.edu/eidol_v2.php). Fig. 2 was produced by smoothing with a 3 × 3 pixel boxcar filter.

A simple estimate for the reality of the association of the various broad-band sources with the Lyα halo can be obtained by looking at the probabilities for their association to occur by chance in a field of background galaxies, as represented by the catalogue of GOODS-S sources of Giavalisco et al. (2004). The three central galaxies A, B and C occur within a $\sim$2.2 × 2.2 arcsec^2 area, matching approximately the projected linear size (along the slit) of the Lyα emission feature. The probability for three or more galaxies with $V < 29$ from the Giavalisco et al. (2004) sample to end up in such a small field by chance, established by randomly positioning 20 000 boxes of that size on a larger 2 × 2 arcmin^2 test area, was found to be 1.0×10^{-3}. Taking a different viewpoint by assuming that the presence of the Lyα halo is always associated with a continuum object and thus fixes the position of the first galaxy, the probability that at least two more galaxies, as observed, occur in the same area turns out to still be as low as 7×10^{-3}.

The membership of additional objects E and F at larger radii cannot be ascertained with the same approach because of the larger volume, larger background density of fainter objects and incompleteness of the Giavalisco et al. (2004) sample, and so the probability of having five objects with luminosities as low as E and F in a 10 × 10 arcsec^2 box is consistent with the background density.

2.2.1 One-dimensional spectra as a function of position along the slit

Fig. 3 shows four one-dimensional spectral slices, with the first three offset by 0.75 arcsec with respect to each other in the direction along the slit (i.e. south–north; the last one has a slightly

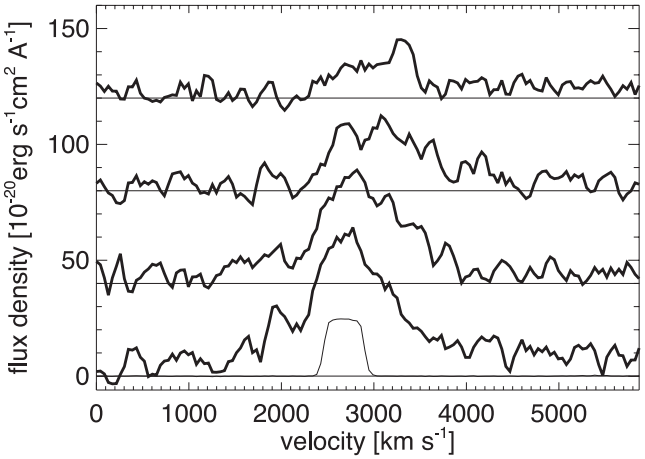

Figure 3. One-dimensional spectra, representing four horizontal cuts through the spectrum in Fig. 1 (with their north–south positions indicated by the white horizontal lines straddling the left-hand and centre panels of Fig. 2). The first three cuts are offset by 0.75 arcsec north with respect to each other, whereas the northernmost one is offset such as to line up with the Lyα finger extending north-east from the main clump. The bottom spectrum is the southernmost cut and roughly lines up with the continuum produced by objects A and C (see Fig. 2 for the nomenclature). The second spectrum from the bottom approximately runs through the northernmost part of the elongated structure 'T2', the third spectrum from the bottom through the object 'B' and the topmost one through 'T3'. The small peak in the topmost spectrum corresponds to the finger of Lyα emission in Fig. 1. The spectra are produced from the two-dimensional spectrum by smoothing with a 1.75-pixel wide Gaussian kernel and extracting a 3-pixel wide box profile. The flux density ordinate refers to the flux density gathered in a 3-pixel wide spectrum. The spectra have been offset by identical amounts along the flux density ordinate for clarity. The thin boxy profile at the bottom is the measured line profile for unresolved emission filling the slit (from a HeNeAr calibration lamp).

smaller offset made to line up with an extended 'finger' of Lyα emission, visible also in Fig. 1). The positions of the spectra along the slit are also indicated in Fig. 2 by the four horizontal lines.

As seen in Fig. 3, the width of the red peak initially appears to change little, going south to north, between the first (southernmost) and third positions. Across the first three slices, the centroid of the line changes only insignificantly, but in the topmost slice the peak of the flux occurs almost 500 km s^{-1} to the red of the peak in the first spectrum, consistent with its position being chosen to spatially intersect the finger of Lyα emission. While a ramp-like remnant of the extended emission peak remains, the peak on top of it, caused by the finger, is now much narrower (FWHM ∼190 km s^{-1}; see also the two-dimensional spectrum in Figs 1 and 2).

The interpretation of the line widths depends crucially on the position of the emitting gas in the direction across the slit. If the Lyα emission is sufficiently spatially extended to fill the slit, then different positions in the direction across the slit amount to noticeable shifts in observed wavelength on the detector. In this case, 1 arcsec west corresponds to 3.32 Å to the red. Thus, the east–west separation between the objects A/C and B alone would shift any Lyα emission from these objects by 250 km s^{-1}, even if there were no velocity difference between the two locations. The full velocity extent across the slit amounts to 460 km s^{-1} FWHM. The actually measured spectral response for an unresolved, spatially extended emission line is shown as the boxy, thin solid line in Fig. 3.

2.2.2 *The puzzle of the discrepant photometric redshifts*

We note that the photometric redshifts for objects A and B from the COMBO-17 (Wolf et al. 2001), GOODS–CFDS–MUSIC (Grazian et al. 2006) and MUSYC (Cardamone et al. 2010) collaborations do not agree well with each other or with the spectroscopic Lyα redshifts (Table 1). The difficulty of separating spatially close objects in the partly ground-based data, their faintness and the presence of Lyα emission in the blue filter may be partly to blame here. However, given our rather peculiar selection criterion (extended, asymmetric Lyα emission) it is conceivable that the underlying objects are also peculiar, in the sense that their broad-band colours may not have been anticipated by the usual photometric redshift techniques. Indeed, object A is unusually bright in the U and B bands for $z = 2.63$ which must have led the surveys to assign a lower redshift than indicated spectroscopically by the Lyα line.

Object 'A' may host an AGN, which, at first sight, may seem consistent with the relatively large line width (870 km s^{-1}) of the emission line. However, the fact that the Lyα emission line width is spatially extended, retaining its spectral line width over several arcseconds in the north–south direction away from the continuum trace of A suggests that this is not the broad emission line of an AGN, which would be spatially compact. Moreover, we have argued above that the line width may be partly caused by the spatially extended emission and the wide slit. There are currently no other signs (high ionization transitions, radio- or X-ray detections) to support an AGN interpretation. The He II 1640 Å region is somewhat damaged in the spectrum and does not allow us to make a meaningful measurement. We note that there is a nearby object ('E', in our table) for which the MUSYC survey (Cardamone et al. 2010) quotes a very similar photometric redshift ($z_{\rm phot} = 2.092$) as for object 'A' ($z_{\rm phot} = 2.066$). The most likely explanation is that A is at the spectroscopic redshift of Lyα (indicated also by a faintly visible Lyα forest decrement in its continuum); that A and E with their similar colours are indeed at the same redshift, and that both photometric redshifts are off by similar amounts. It is conceivable that these are physically similar objects made unusually blue by the same mechanism. Both may have undergone recent starbursts, which may have produced objects brighter in the U and B bands than the templates used for photometric redshift determinations. We have fitted the GOODS–CFDS–MUSIC broad-band magnitudes of object A in the European Southern Observatory WFI $U38$ (hereafter 'U'), *HST*/ACS WFC $F435W$ ('B'), $F606W$ ('V'), $F775W$ ('I') and $F850LP$ ('z') bands with spectral synthesis models of instantaneous starbursts and continuous star formation from the STARBURST99 library (Leitherer et al. 1999). Good fits at the observed Lyα redshift were obtained for a burst with the default input parameters, plus a total stellar mass of 6.7×10^7 M$_\odot$, a metallicity of 0.020 solar and an age of 4×10^6 yr (Fig. 4). Continuous star formation with a star formation rate of 14 M$_\odot$ yr^{-1} observed at a very similar age gave a similarly good representation of the bluer band colours. The rest-frame slope of the ultraviolet (UV) continuum β, with $f_\lambda \propto \lambda^\beta$ determined from the $V - I$ and $U - V$ colours, is $\beta(V - I) = -2.3161$ and $\beta(U - V) = -2.046$, respectively. These continuum colours are rather blue compared to those of known Lyα emitters at similar redshifts (e.g. Venemans et al. 2005) and presumably indicate the absence of dust. With a $\beta < -2$ the object appears similar to the less evolved

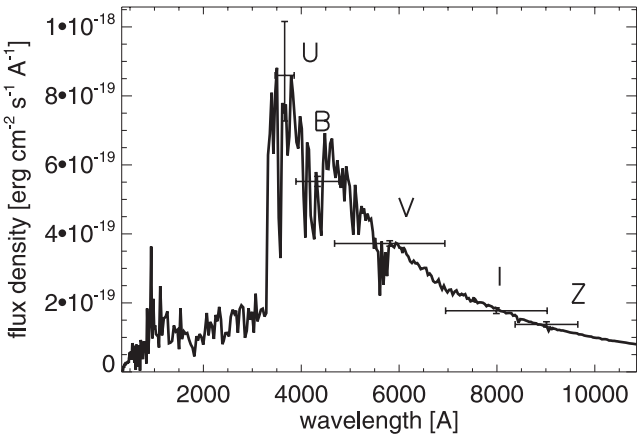

Figure 4. Best fit of the broad-band measurements for galaxy A with filters WFI *U*38, and *HST*/ACS *B*, *V*, *I* and *Z* from Grazian et al. (2006) using a STARBURST99 model spectrum (Leitherer et al. 1999), with total stellar mass 6.7×10^7 $M_\odot$ and age 4×10^6 yr, redshifted to $z = 2.63$ and attenuated by the average Lyα forest opacity blueward of 1215.67 Å in the rest frame.

star-forming objects observed at redshifts possibly associated with the epoch of reionization (e.g. Bouwens et al. 2010; Finkelstein et al. 2010; Dunlop et al. 2012).

The formation of such a young stellar population may have been triggered by the interactions between the members of the proto-galactic group. Gas-dynamical disturbances and rapid star formation would naturally lead to enhanced and messy Lyα emission, with obvious similarities to the earlier case discussed in Paper I. If the galaxies entered their future common halo with a pre-existing stellar population, the interaction would lead to a composite population with the young stars superposed on that older stellar population. An attempt at extracting the properties of the older stars by fitting the observed broad-band magnitudes with the MAGPHYS SED fitting software (da Cunha, Charlot & Elbaz 2008), using a larger set of filters including the *U*, *B*, *V*, *I* and *z* used with STARBURST99 plus rest-frame optical VLT *H*, *J*, *K* and *Spitzer* Infrared Array Camera 3.6, 4.5 and 5.8 μ data as collated by the GOODS–MUSIC collaboration (Grazian et al. 2006), yields a stellar population of 1.1×10^9 $M_\odot$ with formation age 7×10^8 yr. Omission of the *U* and *B* filters (which are not well fit) produced no changes in the parameters from the MAGPHYS output but shrank the reduced χ^2 from 1.30 to 1.04. Thus, the MAGPHYS SED fitting of the rest-frame optical colours is picking up the older population of object A, dating from before the recent star formation event.

2.3 Broad-band detection of a Lyα emitting filament

Further insights into the physical state of the halo are provided by the presence of the faint, filamentary thread of emission (marked 'T2') in the *B*-band exposure, shown in the central panel of Fig. 2. The thread appears to extend continuously from (03:32:38.800 −27:44:28.5) to (03:32:38.631 −27:44:28.99), i.e. over 2.3 arcsec (18.7 h_{70}^{-1} kpc proper). Its width can be traced over about 4 pixel or 0.12 arcsec and so it may be spatially unresolved in the short dimension. It terminates at either end in brighter spots, of which at least the western (brighter) one (object F) contains stars as it is visible in both *B* and *V* bands. This filament is only partly covered by our slit, but its position along the slit is consistent with it being co-spatial with the Lyα emitting region, at least in projection. Its apparent connection with a galaxy makes it unlikely that the filament is an artefact caused by the instrument or by the data reduction. It is possible that the filament is a chance coincidence in projection with a foreground or background object unrelated to the Lyα emitter. It is difficult to estimate the probability of this occurrence, as the range of variability in the appearance of such structure that would be recognized by eye as a 'filament' is hard to know. We have searched by eye for similar filamentary structure, including a leading knot of emission, in a larger 2×2 arcmin^2 region of the GOODS-S *B*-band image, centred on our object and found 15 structures that fit the bill, suggesting that the Poissonian probability of having a chance coincidence of such a structure in a 5×5 arcsec^2 area centred on the Lyα emitter is a $\sim 6\sigma$ excursion.

The filamentary structure is remarkable in that it is absent from the (deeper) *V* band (and not visible in any of the other ACS bands either). We measured the flux in an irregular aperture drawn tightly around the filament. The sky background and the noise were measured from offset background windows placed in apparently clean areas of the image. The measured sky-subtracted fluxes in the filamentary aperture in the GOODS ACS mosaic *B*- and *V*-band images amount to 0.151 ± 0.032 counts (*F*435*W*) and -0.0979 ± 0.0654 counts (*F*606*W*), i.e. the filament is a 4.7σ detection in the *B* band and a non-detection in the *V* band.

Using the published ACS GOODS zero-points of 25.67 (*F*435*W*) and 26.49 (*F*606*W*), we obtain AB magnitudes for the filamentary aperture of 27.73 (*F*435*W*) and >29.44 (1σ; *F*606*W*), or a 1σ upper limit $B - V = -1.71$. Interestingly, the wavelength of the Lyα, if at the redshift of the main halo, falls close to the central wavelength of the *B* filter (transmission 92 per cent). Thus, the very blue colour may be caused by a dominant contribution from Lyα emission to the broad-band count rate. More precisely, if the flux were indeed Lyα, then the width of the *B* filter would limit the redshift of the filament to be within $2.2 < z < 2.9$, which is consistent with it belonging to the same halo as the spectroscopically detected, main Lyα emission. We can estimate the hypothetical Lyα flux from the $B - V$ difference, assuming that the underlying stellar population is similar to colour-selected ('Lyman break') galaxies (e.g. Shapley et al. 2006) in that its continuum is essentially flat in f_ν. Ascribing the flux in the *B* band to the sum of line ($f_\nu^{\mathrm{Ly}\alpha}$) and continuum ($f_\nu^{\mathrm{cont}}$) emission and the flux in the *V* band (or rather the upper limits) entirely to continuum emission, we can then write

$$f_\nu^{\mathrm{Ly}\alpha} = \left\langle f_\nu^B \right\rangle - \left\langle f_\nu^{\mathrm{cont}} \right\rangle \approx \left\langle f_\nu^B \right\rangle - \left\langle f_\nu^V \right\rangle , \qquad (1)$$

where it has been assumed that the flux per frequency interval is flat between *B* and *V*.

The resulting total Lyα flux $F_{\mathrm{Ly}\alpha}$ responsible for the observed $B - V$ counts can then be estimated from

$$\left(\left\langle f_\nu^B \right\rangle - \left\langle f_\nu^V \right\rangle \right) \approx F_{\mathrm{Ly}\alpha} \lambda_{\mathrm{Ly}\alpha} T_{\mathrm{Ly}\alpha}^B \left(c \int \frac{T_\lambda^B}{\lambda} \mathrm{d}\lambda \right)^{-1} \qquad (2)$$

as $F_{\mathrm{Ly}\alpha} = (4.0 \pm 1.2) \times 10^{-17}$ erg cm^{-2} s^{-1}. Here, T_λ^B is the transmission of the *B* filter, and the additional λ terms in the integrals account for the fact that the count rate is proportional to λf_λ. The total flux from the filament in the *B* band is somewhat larger than the total Lyα flux in the spectrum that has passed through the spectrograph slit. However, the filament is mostly outside of the slit, so the Lyα line in the spectrum is only partly due to the filament and the contribution of the filamentary emission may not dominate the spectroscopically observed emission.

An assessment of the equivalent width is very uncertain because of the asymmetric and non-linear errors as we do not have a detection of the continuum, but we can get an idea of the uncertainties involved by trying to maximize the uncertainties in a correlated way such as

to favour as low an equivalent width as possible. At the 1σ level, if we simultaneously subtract a 1σ deviation from the *B*-band flux and add such a deviation to the *V*-band flux (and instead of the formally negative flux we conservatively impose a positive *V*-band flux with the size of a 1σ error), we find that such fluctuations would result in a rest-frame equivalent width lower limit of 688 Å (1σ). If we had used only the error in *V* but assumed a 3σ fluctuation, the allowed rest-frame equivalent width would still be 149 Å. It is clear however that the data are also consistent with no stellar continuum, and the much higher upper bound on the equivalent width given by the two-photon continuum (e.g. Dijkstra 2009).

We briefly point out the presence of another faint patch of emission, shown as 'T3' in Fig. 2, that is also visible in the *B* band but not in the *V* band, with a 3σ upper limit on the $B-V$ colour of <-1.6. Unlike the filament T2, this structure is not connected to any other object so we have less reason to consider it as real or as belonging to the halo, other than it being a 7.9σ detection above the background noise. It lines up well, however, in the direction along the slit with the narrow 'finger' of Lyα emission seen in the two-dimensional spectrum (Fig. 2; see the uppermost two spectral cuts). If the *B*-band light were dominated by Lyα flux, the resulting rest-frame Lyα equivalent widths indicated by the upper limits on the *V*-band flux would be between 426 Å (3σ) and 1768 Å (1σ), again assuming a flat spectrum. Increasing the contribution of a hypothetical stellar continuum to the *B* band by changing the continuum slope $\beta(B-V)$ from flat ($=-2$) to an extreme value of -4, would only increase the $B-V$ by 0.6. If the *B*-band light for T3 were entirely due to Lyα flux, the flux would be $(8.3\pm1.5)\times10^{-17}$ erg cm^{-2} s^{-1}, whereas the spectroscopically observed fraction of the flux in the region of the two-dimensional spectra that coincides with the T3 structure in projection is about 1.2×10^{-17} erg cm^{-2} s^{-1}. T3 straddles one of the slit jaws, so much of the light may not fall on to the slit. The crude assumption that the slit losses amount to 2/3 of the flux would correct the total spectroscopically detectable flux to 3.6×10^{-17} erg cm^{-2} s^{-1}. This is within about 3σ of the flux in the *B* band. We conclude that it is possible that the apparent *B*-band flux in the region T3 may be real Lyα emission, partly seen in the spectrum as well. The Lyα 'finger' visible in Figs 1 and 2 that appears to correspond to the T3 emission shows up in the one-dimensional cuts (Fig. 3, top spectrum) as the little narrow peak near 3400 km s^{-1}. The small line width (190 km s^{-1} FWHM) implies that the source does not fill the slit, and the single, symmetric, narrow line may reflect optically thin (i.e. partly ionized) gas.

2.4 Sources of the observed Lyα emission

In this section we look at the observed Lyα budget, distinguishing between the total flux observed spectroscopically through the slit, and the presumed flux from the extended components T2 and T3 as seen in the *B*-band imaging.

For the *total spectroscopically observed Lyα flux* to be produced by the stellar sources present, the ionizing photons expected from the rest-frame 1500 Å luminosity L_{1500} of the broad-band objects have to be able to provide the photoionization rate required. Estimating the stellar yield of ionizing photons same as in Paper I for the three brightest $z\sim2.63$ sources A, B and C, we arrive at $\dot{N}_*^{\rm ion}=6.6\times10^{53}$ s^{-1}, whereas the production rate required by the observed Lyα emission is $\dot{N}_*^{\rm Ly\alpha}=2.0\times10^{53}$ s^{-1}, about 30 per cent of the stellar rate, so the number of ionizations needed to account for the overall Lyα flux that went through the spectrograph slit can be accounted for as photoionization from the stellar sources thought to be associated with the Lyα halo.

The astrophysical source of the *filamentary Lyα emission* is not immediately obvious. Below we will discuss several possibilities, including fluorescence in response to ionizing radiation from one of the nearby galaxies, or from an obscured AGN; cooling radiation in a cold accretion filament; shocks and emission from wind shells; and intrahalo star formation, including special conditions like more massive or metal-poor stars favouring large yields of Lyα and ionizing photons.

2.4.1 *Fluorescence caused by the loss of ionizing photons from one of the other galaxies in the halo*

The filamentary Lyα may be caused by fluorescence in response to ionizing photons from galaxy A. As this was the preferred explanation for the earlier, Rauch et al. (2011) object, we will consider it briefly here as well. Using the same assumptions as in that paper, the number of ionizations required to occur in the filament, if produced by escaping, stellar, ionizing radiation from galaxy A, at a projected distance $R=16.6$ kpc from the centre of the filament, require A to have a luminosity density L_{1500} of

$$L_{1500}^{\rm A}=4.7\times10^{30}\ {\rm erg\ s^{-1}\ Hz^{-1}}\left(\frac{F_{\rm Ly\alpha}}{4\times10^{-17}}\right)\times\left(\frac{1}{1-f_{\rm esc}^{\rm ll}}\right)\left(\frac{1}{f_{\rm esc}^{\rm Ly\alpha}}\right)\left(\frac{R}{16.6\,{\rm kpc}}\right)^2\left(\frac{\Delta A}{18.7\,{\rm kpc}^2}\right)^{-1}. \quad (3)$$

Here it was assumed that two-thirds of the ionizing photons get converted into Lyα, and we have computed the number of ionizations in terms of the escape fraction for ionizing photons, $f_{\rm esc}^{\rm ll}$, the escape fraction for Lyα photons, $f_{\rm esc}^{\rm Ly\alpha}$, and the area ΔA subtended by the filament. The actual observed luminosity density, based on the magnitude $m_{\rm AB}(1600\,{\rm Å})=24.84$ falls short by a factor of 70 of achieving this ionizing flux at the (projected) position of the filament, even if all the escape fractions take on their most optimistic values. Similar conclusions are obtained from the STARBURST99 models of object A, where the instantaneous, 4×10^6 yr old starburst falls short of producing the required yield of ionizations by a factor of 67. The continuous star formation model with 14 M$_\odot$ yr^{-1} produces more ionizing photons but still falls short by a factor of 22. Stellar winds may be able to increase the escape of ionizing photons from stellar atmospheres by an order of magnitude (e.g. Najarro et al. 1996), but that may still not be sufficient.

The possibility that object A (or any of the other galaxies) could harbour an AGN that would irradiate the filament with ionizing photons cannot be ruled out. Fluorescence induced by an AGN may cause very large equivalent widths over distances much larger than considered here (e.g. Cantalupo, Lilly & Haehnelt 2012). As mentioned above, the spectral line width of the Lyα line at FWHM $=870$ km s^{-1} is somewhat large for a standard Lyα emitter, but the broad emission is spatially extended, and so does not in itself suggest that the galaxy hosts an AGN. However, the non-detection of this object in the *Chandra* X-ray data puts limits on the nature of the underlying source. Luo et al. (2010) report a detection threshold for the soft X-ray band ([0.5–2.0] keV) of 1.9×10^{-17} erg cm^{-2} s^{-1}. Extrapolating the flux in that band to the total flux of hydrogen ionizing photons below the Lyman limit would require a very steep slope of $f_\nu\propto\nu^{-\alpha}$ with $\alpha\sim3.3$, in order to produce 4×10^{55} s^{-1} of ionizing photons. The AGN could be Compton-thick and emit no X-rays along the line of sight to the observer, while still irradiating the filament. For an AGN with intrinsic luminosity density (in units

of erg s^{-1} Hz^{-1}) of $L_\nu \propto \nu^{-0.5}$ for $\lambda < 1050$ Å, and $L_\nu \propto \nu^{0.5}$ for $\lambda > 1050$ Å (following Bolton & Haehnelt 2007), capable of inducing the observed Lyα flux in the filament through an optically thin sightline, the unextinguished apparent AB magnitude in the ACS *F*435*W B* band would be 23.8, brighter by about 1.5 mag than the observed *B*-band flux of galaxy A. Given that only about 1 per cent of all Lyman break galaxies according to the standard definition are QSOs, one would expect to find a QSO on our long slit with a Poissonian probability of about 4 per cent. We have, however, already another QSO on the slit (to be published in a future paper). The probability for finding two or more QSOs in the same volume is 0.15 per cent.

2.4.2 *Shocks and emission from wind shells*

Shocks, and the emission from wind shells (e.g. Taniguchi & Shioya 2000; Mori, Umemura & Ferrara 2004), are further candidates for high equivalent width emission from narrow structures and could provide Lyα emission through either collisional or photoionization channels. Paper I considered the possibility of shocks ionizing the neutral hydrogen in the $z = 3.34$ emitter, but found them unlikely to explain the observed Lyα emission, as a rather large shocked area and high velocities were required. A similar situation exists here, with the Lyα emitting region of the filament having a much smaller area. We have no observations of shock diagnostics (e.g. the He II 1640 Å line) available, nor does the filamentary geometry suggest a shell or shocked sheet of gas. In the starburst models discussed above (4×10^6 yr old instantaneous starburst or continuous star formation), the mechanical energy from O and B and Wolf–Rayet stars (Leitherer, Robert & Drissen 1992), if disposed of in the form of Lyα radiation, could give a significant boost to the total Lyα emission from an underlying stellar population, but not a dominant one.

2.4.3 *Emission from cold gas accretion, powered by cooling radiation*

The filament in the present halo shows certain similarities with the $z = 3.34$ filament discovered in the Rauch et al. (2011) object. Both terminate in a faint galaxy, and – if we accept the premise that the flux in the *B*-band image of the present case is indeed mainly Lyα emission – neither can be linked causally to any stellar features. The possibility can again be raised whether this is actually one of the predicted cold stream filaments thought to dominate the accretion process at early times and for lower mass galaxies. Paper I suggested that the filamentary structure seen near the $z = 3.34$ galaxy is likely to be seen in fluorescence when exposed to ionizing external radiation from the main galaxy (or possibly a hidden AGN therein, or a tidal tail leaking ionizing photons), but such an explanation may be somewhat less likely in the present case because of the high surface brightness of the filament. Global, extended cooling radiation from a relatively low-mass halo like the present one (see below) may disfavour a signal strong enough to be detected (e.g. Haiman, Spaans & Quataert 2000; Fardal et al. 2001; Dijkstra & Loeb 2009), but the radiation may be detectable if it comes from very compact regions, and the partly neutral cores of individual filaments may actually be visible at current sensitivity levels. Faucher-Giguère et al. (2010), Goerdt et al. (2010, 2012) and Rosdahl & Blaizot (2012) have studied Lyα emission from cold accretion filaments, with a focus on predicting the emissivity. These studies agree in that the densest regions of the filaments should be partly neutral, and their Lyα emission should be dominated by collisional excitation cooling. If we take the observed filament as a $z = 2.63$ cylinder of overdense gas with a length of 16.6 kpc (omitting the region of the apparent galaxy 'F' at the tip) and a diameter of 1 kpc, the Lyα flux produced by collisional cooling radiation at the peak emissivity ($10^{-11.2}$ photons cm^3 s^{-1}, near $T = 20\,000$ K, e.g. as given by Faucher-Giguère et al. 2010) can be written as

$$F_{\mathrm{Ly}\alpha} = \left(\frac{\dot{E}V}{4\pi D_{\mathrm{L}}^2}\right) = 1.1 \times 10^{-25} \left(\frac{\epsilon_{\mathrm{Ly}\alpha} n_{\mathrm{H}}^{-2}}{10^{-11.2}\,\mathrm{cm^3\ s^{-1}}}\right) \times \left(\frac{n_{\mathrm{H}}}{1.3 \times 10^{-5}}\right)^2 \mathrm{erg\ cm^{-2}\ s^{-1}}, \quad (4)$$

where $\dot{E}$ is the emissivity (erg cm^{-3} s^{-1}), V is the volume of the filament, D_{L} is the luminosity distance and $\epsilon_{\mathrm{Ly}\alpha}/n_{\mathrm{H}}^2$ is the emissivity of Lyα photons, divided by the square of the total hydrogen density (photons cm^3 s^{-1}) in the nomenclature of Faucher-Giguère et al. (2010). We find that the observed flux from the filament, 4×10^{-17} erg cm^{-2} s^{-1}, could be produced by collisionally cooling gas with a total hydrogen density of 0.24 cm^{-3}, if a steady supply of potential energy can keep the gas at the optimum temperature. Thus, at such densities, which are at the high end of the expected density range for cold streams, cooling radiation may at least in principle be a viable explanation because of the compactness of the filament.

2.4.4 *Intrahalo star formation, by young and metal-poor stars*

Alternatively, intrinsic star formation in the filament may be able to produce enough ionizing photons to explain the observed Lyα line strength. Large Lyα equivalent widths of the order of a couple of hundred Å and beyond have been reported previously for Lyα emitting galaxies (e.g. Kudritzki et al. 2000; Malhotra & Rhoads 2002; Saito et al. 2006). To explain the large equivalent widths through stellar photoionization requires the stellar population to be hot, young and metal poor (e.g. Kudritzki et al. 2000; Tumlinson & Shull 2000; Schaerer 2002; Tumlinson, Shull & Venkatesan 2003), or to exhibit a top-heavy initial stellar mass function (IMF; e.g. Malhotra & Rhoads 2002). Under such circumstances, stellar yields of ionizing photons and the conversion of ionizations into Lyα line photons (through departures from case B) can be strongly enhanced (e.g. Raiter, Schaerer & Fosbury 2010; Inoue 2011), even much beyond the 150–700 Å range suggested here. In fact, the presence of a young population (4×10^6 yr) at least for the starburst of galaxy A is consistent with these models. The blue $B - V$ colours observed for some of the galaxies also agree well with the colour range expected of very metal-poor, possibly Population III stars (Jimenez & Haiman 2006). However, a filament of length L, if not formed simultaneously as in the case of a compressed shell or caustic, would be subtended with a relative velocity v, e.g. by star-forming regions trailing or forming behind the galaxy F. Such a protracted unfolding of an extended star-forming filament would produce an age difference between head and tail of

$$t = 8.1 \times 10^7 \left(\frac{L}{17\,\mathrm{kpc}}\right) \left(\frac{v}{200\,\mathrm{km\,s^{-1}}}\right)^{-1} \mathrm{yr}. \quad (5)$$

This is a factor of ∼20 longer than the age of the young stars we have postulated to be present throughout the filament at the time of the observation, so the fact that the filament is visible at similar surface brightness throughout its length is a puzzle. It is of course possible that the conditions for the continuous formation of stars causing strong Lyα emission simply persist for the entire observable lifetime

of the filament. Another possible explanation may be found in the finite H I recombination time-scale. Assuming an electron density N_e, recombination coefficient α_{rec}, a gas temperature of 2×10^4 K, a largely ionized medium and a density of the emitting filament of 180 times the mean density of the Universe at the observed redshift (this is equivalent to assuming that the halo has collapsed recently), the recombination time-scale of the gas in the filament

$$\tau_{rec} = (N_e \alpha_{rec})^{-1} \sim 5.4 \times 10^7 \text{ yr} \left(\frac{1+\delta}{180} \right) \quad (6)$$

can be of a similar order of magnitude as the likely age of the filament, so even a wave of short-lived star formation travelling with the tip of the tidal tail would lead to an extended period of recombinations and visibility of Lyα emission. If a short instantaneous starburst is to blame for the photoionization, then the combination of a finite recombination time-scale with the rapid decline in the stellar broad-band light would assure that the observed equivalent width would be very large, similarly large as expected if produced by the more exotic star formation scenarios considered here (see Appendix A).

The dynamical origin of the filament T2 may be understood in analogy with low-redshift observations of interacting galaxies. The presence of an apparently tidal stellar feature (T1) near object A may suggest that the filament is a tidal tail, too. Object F could be the remnant of one of the interacting objects, or a dwarf galaxy that has formed at the tip of the tidal tail, as has been proposed for low-redshift interacting galaxies (e.g. Schweizer 1978; Mirabel, Dottori & Lutz 1992). Young stellar populations in star-forming clumps along low-z tidal tails have also been observed and studied in considerable detail (e.g. Whitmore & Schweizer 1995; Smith et al. 2008; Karl et al. 2010).

In an intriguing alternative scenario, the luminous tail may be gas stripped from object F by ram pressure when passing through the IGM, and the increased turbulence may have led to in situ star formation. Such a phenomenon may have been observed in the low-redshift intracluster medium (e.g. Yoshida et al. 2008, 2012; Hester et al. 2010) and is consistent with current theoretical ideas (e.g. Kapferer et al. 2008; Tonnesen & Bryan 2010, 2012), although, as far as we know, there are no studies of such an effect at the level of an individual galactic halo, and at high redshift. Intriguingly, the presence of metal-poor stars may directly reflect an inflow of low-metallicity gas from the ambient IGM/halo gas ($\log Z/Z_\odot \sim -2.8$ at $z \sim 3$; Schaye et al. 2003; Simcoe, Sargent & Rauch 2004, with pockets of lower metallicity persisting at the same redshifts; Fumagalli, O'Meara & Prochaska 2011b), favouring the formation of metal-poor stars even at relatively late times.

And finally, the astrophysical scenarios just described, namely the presence of low-metallicity, hot, young stars in the low-opacity environment of the gaseous halo, would lead to an enhanced production and escape of ionizing radiation, favourable properties for the (so far hypothetical) galactic sources required for the reionization of hydrogen.

3 OVERALL NATURE OF THE UNDERLYING HALO

3.1 Halo membership

As shown above, the association of at least three objects A, B and C with the Lyα emission is statistically highly unlikely to have occurred by a chance coincidence. In addition, its Lyα forest decrement indicates that A is at the same redshift as the Lyα emission. Object C is very close to A in projection and similar to A in colours, and may also be responsible for some of the substructure seen in the Lyα emission.

Because of the faintness of the galaxies, and their larger distance from the halo centre, membership of the other individual galaxies in the halo hosting the Lyα emission cannot be established beyond doubt for all objects. Object F looks like a halo member because it appears physically connected to the filament T2, the emission of which, assuming the object is real, is most plausibly interpreted as Lyα close to the redshift of the main halo.

Object E, as the most distant candidate has similar colours and a similar deviant photometric redshift as A, so it is possibly also belonging to the group.

Keeping in mind the considerable scatter in the relation between stellar and total halo masses, we may identify A with the main halo galaxy and try to gain a crude idea of the halo mass associated with the stellar mass of A. Taking the $1.1 \times 10^9\,M_\odot$ inferred from the rest-frame optical colours using MAGPHYS (see above) as the stellar mass (this ignores the recent starburst), we use the relations between stellar and halo mass derived by Behroozi, Conroy & Wechsler (2010) (extrapolating to $z = 2.63$) and arrive at a total halo mass of $10^{11.6}\,M_\odot$. We cannot determine the stellar masses for the faint satellites because of a lack of data in the infrared (except for A), but we assume very crudely that a factor of ∼10 difference between the z-band fluxes of the brightest object A and the faintest object F reflects a decade in halo mass ratios. Then the expected number of satellites (e.g. Kravtsov et al. 2004) for this case are quite consistent with a group of 4–5 members in a $\sim 10^{12}\,M_\odot$ halo, as suggested by the observations.

3.2 Faint, extended emitters and Lyα blobs

As for the distinction between our asymmetric haloes and those hosting the bright extended emitters known as Lyα blobs, it may be primarily one of mass, with our emitters being single, protogalactic haloes, and the blobs being more akin to the progenitors of galaxy clusters (e.g. Yang et al. 2010). In the more massive haloes, the larger number of subhaloes and the wider variety of sources capable of producing Lyα emission renders the nature of Lyα blobs more diverse and adds considerable complexity (e.g. Yang et al. 2011; Bridge et al. 2012; Prescott et al. 2012). The detection of He II 1640 Å emission in these objects (e.g. Scarlata et al. 2009; Prescott et al. 2012) also strongly points to some non-standard stellar or non-stellar ionization mechanism, and the finding of a diffuse stellar component (Prescott et al. 2012) may just be one of the consequences of the multiple interactions we appear to be seeing individually in the smaller haloes.

3.3 Faint, extended emitters and more typical Lyα emitting galaxies

It is instructive to look at the differences in the appearance of the Lyα emission line and other parameters between the extended Lyα emitters found by Paper I and in the present study, and those 'standard' Lyα emitters that dominate typical Lyα emitter samples. The latter, discovered by broad-band colour-selection or narrow-band imaging, generally are more highly peaked in the spatial direction. For comparison, we show, in Fig. 5 our two extended emitters (left-hand panels) and two bright, compact Lyα emitters (right-hand panels) that happened to be accidentally intersected by the long slit during the Keck LRIS blind survey in the HDFN (Rauch et al., in preparation). Colour- and luminosity-wise, the latter two

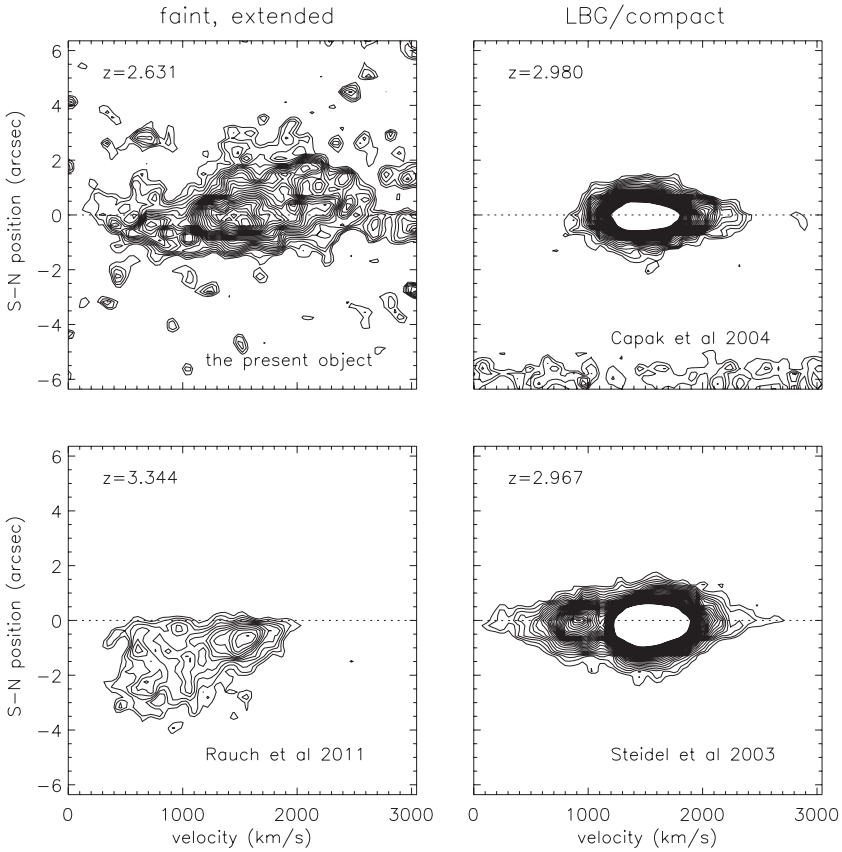

Figure 5. Comparison between the two extended emitters (the $z = 2.63$ object at the top left; the Rauch et al. 2011 $z = 3.34$ object at the bottom left) and two galaxies that qualify as 'Lyman break' galaxies with Lyα emission, from a Keck LRIS survey in the HDFN and its immediate vicinity (Rauch et al., in preparation). The spectra have been resampled to match the dispersion and spatial scale, with the LDSS3 HUDF spectra (left-hand panels), and were smoothed in both directions to match the coarser pixel resolution of the binned LRIS HDFN data (right-hand panels). The spectra were put on the same flux contour scale, with the lowest and highest flux density contours corresponding to 2.1×10^{-20} and 2.4×10^{-19} erg cm^{-2} s^{-1} Å^{-1}. The dotted lines give the approximate position of the peak of the continuum traces. The images are centred in the dispersion direction on the peak emission, as the systemic redshifts are unknown. The spectra of the compact objects on the right-hand side show the usual red peak with a sharp drop on the blue side and an extended red shoulder. Absorption troughs in the continuum just blueward are present but not visible in this contour plot. The bottom system has a (partly suppressed) blue peak as well.

[J123647.09+620935.8 (Capak et al. 2004) at $z = 2.9804$, top right-hand panel, and J123646.94+621226.1 at $z = 2.96707$, also known as HDF0D10 (Steidel et al. 2003); bottom right-hand panel] can be classified as Lyman break galaxies with Lyα emission. The objects are presented on the same spatial, velocity and flux scale so that a direct comparison can be made. In addition, Fig. 6 shows the two profiles from the right-hand column of Fig. 5, collapsed along the dispersion direction. These profiles correspond to the projections of the central parts of the surface brightness profiles that have passed through the slit. The solid profiles show the Lyα emission after the continuum (measured immediately to the red of Lyα) has been subtracted. The continuum profile itself (dotted line), scaled for comparison to the same peak value, outside of the central arcsecond is clearly less extended than the Lyα emission which can be traced out to about 2 arcsec at the present sensitivity. The two objects also show small spatial shifts between Lyα and continuum emission of the order of a (binned) 0.27-arcsec wide pixel, or about 2 kpc proper, and the profiles appear mildly asymmetric. The finding of extended Lyα haloes even around these very compact individual galactic sources is consistent with the individually detected, extended profiles found (for generally fainter) objects in the somewhat deeper VLT–FORS survey by Rauch et al. (2008), and has also been seen in stacks of Lyman break galaxies (Hayashino et al. 2004; Steidel et al. 2011). The difference between the extended, asymmetric profiles on the left of Fig. 5 and the compact, more-or-less symmetric ones of the Lyman break galaxies on the right, may have, as we have argued earlier, several causes that are likely to be related to the hierarchical nature of the assembly of the haloes. Clustering of galaxies will lead to multiple sources spatially spread out over the extent of the halo. The increased differential motion of the gas stirred by the infalling galaxies will open up escape channels in velocity space for Lyα line radiation. Galactic collisions may inject stellar tails into the lower opacity gaseous halo, and, in conjunction with the ambient gas pressure perhaps strip them partly of the ambient interstellar medium. Interactions may temporarily produce physical holes in the gaseous haloes through which Lyα and ionizing radiation may be able to escape. Star formation may be triggered by merger-induced infall and gas-dynamical instabilities in the gaseous halo. Thus both forms of Lyα emitters may just represent different stages in the formation of a galactic halo, with the more spatially compact emitters perhaps representing the quiescent phases between interactions, where a single, compact stellar source of ionizing photons dominates the production of ionizing photons and results in a 'compact' source of Lyα emission.

To test the idea that the central few arcseconds of the compact Lyα emitters are dominated by compact sources of ionizing

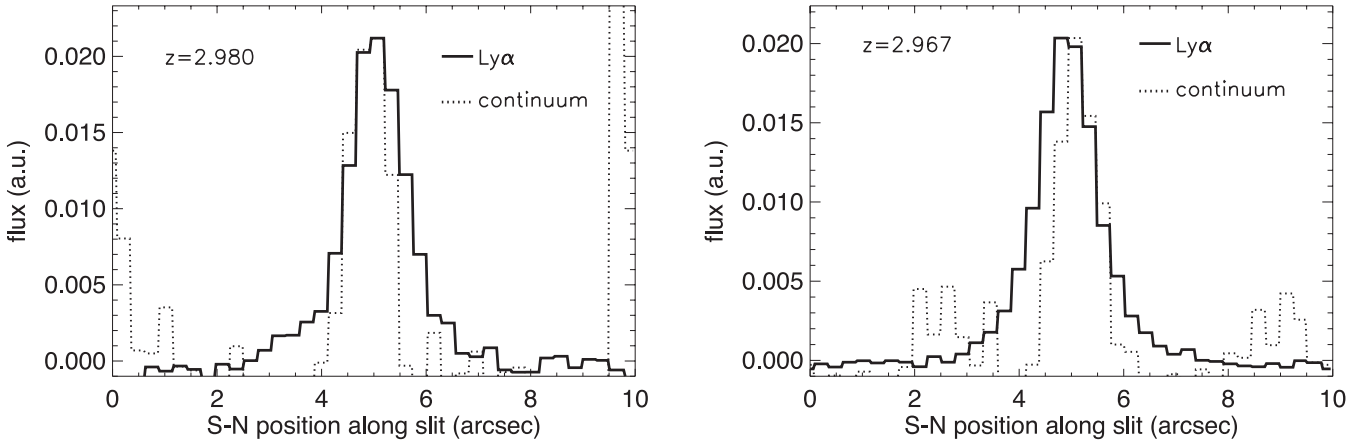

Figure 6. Spatial flux profile along the slit direction, of the two compact Lyman break galaxies J123647.09+620935.8 (left) and J123646.94+621226.1 (right) from Fig. 5. The Lyα spectral profiles (solid lines) were added up along the dispersion direction, and are shown after the continuum as measured immediately to the red of the Lyα emission line (dotted line) has been subtracted. The Lyα line and the continuum are both scaled to have the same peak flux to facilitate a comparison between their respective spatial profiles. While the emission in both is strongly peaked, the Lyα emission has significantly broader wings that can be traced out to about 2 arcsec at this sensitivity level. There is also some asymmetry in that the Lyα and continuum profiles do not line up precisely but are displaced spatially along the slit by shifts of the order of a pixel (0.27 arcsec).

radiation, we take advantage of the fact that the two profiles shown in Fig. 6 are among the deepest spatially resolved spectra ever obtained of Lyα emitters, allowing us to compare them individually to model predictions of the surface brightness profile of Lyα emitters. The outcome of this comparison, described in Appendix B, suggests that single, compact sources of ionizing photons in haloes with moderate expansion velocity (of the order of 100–200 km s^{-1} in the innermost 10–20 kpc) can formally produce spatial Lyα emission surface brightness profiles as compact as observed. The Lyα emission profiles examined here do not show signs of the much larger velocity gradients observed in the absorption troughs of Lyman break galaxies (e.g. Steidel et al. 2011), nor do they seem to be consistent with large wind shells as sources of Lyα emission (e.g. Verhamme et al. 2008), as these would produce much shallower surface brightness profiles than observed.

4 CONCLUSIONS

Based on an ultra-deep long-slit survey of the HUDF and flanking GOODS-S field for faint Lyα emission, we have found a second extended, asymmetric $z = 2.63$ emitter, in addition to the one described in Paper I. The Lyα emitting region coincides spatially with several objects detected in broad-band *HST*/ACS images from the GOODS survey. Multiple photometric redshifts for some of the objects from the literature disagree not only among each other but also with the spectroscopically determined redshift for the Lyα emission. However, the brightest galaxy, A, shows a Lyα forest decrement as expected for the $z = 2.63$ redshift. The rest-frame UV colours of this object are best fit with a very young starburst which may have compromised previous photometric redshift determinations. Several other objects have similar $B - V$ colours. Interactions between the merging progenitors in a common, Milky Way sized halo may account for several unusual findings, including the sprawling Lyα emission, the spatially irregular stellar components, the blue colours and likely presence of young stars in several objects, and evidence for a possibly Lyα emitting filamentary structure connected to a faint continuum source. The 17 kpc long filament (which is mostly outside of the spectrograph slit), and another more diffuse emission region that coincides with a narrow finger of Lyα emission seen in the two-dimensional spectrum, are detected by their excess light in the *B* band, but not in any other broad-band. If the excess radiation is interpreted as Lyα emission, the resulting large inferred equivalent widths either suggest non-stellar processes like Lyα fluorescence, cooling radiation from a cold accretion filament, or the formation of otherwise undetected hot, metal-poor stars, perhaps in a tidal tail or the wake of a ram-pressure-stripped galaxy. Unlike the case of the Rauch et al. (2011) $z = 3.34$ galaxy, where a gaseous filament falling in to the main galaxy appeared to fluoresce in response to ionizing radiation escaping from the same galaxy, the non-detection of sufficiently powerful stellar or AGN sources in the present case disfavours the possibility of fluorescence as the source of the filamentary Lyα. Cooling radiation in a dense, cold accretion stream may give an energetically feasible explanation for the filamentary Lyα. However, the linear structure and trailing appearance of the filament resembles the features seen in low-redshift tidal tails, or the formation of stars in a turbulent, stripped wake, trailing a satellite galaxy moving through the main common gaseous halo.

In the present case, other than through the possible detection of optically thin Lyα emission in the Lyα 'finger', we have no direct evidence for the escape of ionizing radiation, which, because of the low redshift and faintness, may be hard to obtain observationally. However, physical circumstances in an interacting halo should be quite favourable for the escape of ionizing photons. Interaction between halo members may cause disturbances in the gaseous halo and intrahalo star formation in tails and wakes, either of which serves to reduce the opacity for ionizing radiation. The formation of preferentially hot, metal-poor stars, perhaps fed directly by the low-metallicity IGM in the halo, would be characterized by a higher yield of ionizing photons, with a harder spectrum. Interactions, triggering these processes increase rapidly when going towards higher redshift. All these features go in the same direction, suggesting *disturbed galactic haloes may be important contributors of ionizing photons during the epoch of reionization*.

We have briefly discussed the difference between these extended, asymmetric emitters, and other classes of Lyα emitters. Observational samples, irrespective of how they were obtained, tend to be dominated by spatially symmetric, compact sources. Examining two bright Lyα emitting Lyman break galaxies we show that, nevertheless, even those objects have extended Lyα envelopes surrounding the continuum sources of ionizing photons. Comparison

with simple models shows that the observed Lyα surface brightness profiles can be modelled by embedding single point sources of ionizing photons in intact spherically symmetric H I haloes. Very extended stellar sources are not indicated, and radiating wind shells appear inconsistent with the profiles, at least on the $\sim$20 kpc scales that we can observe. We interpret these 'standard' Lyα emitters as haloes in the 'off' stage, where one galaxy strongly dominates the emission and interactions are not currently important. The differences between our faint, extended emitters and the more luminous, rarer Lyα blobs may mainly depend on mass and energetics, with the blobs being more massive haloes containing a larger variety of more powerful sources of Lyα radiation like AGN and radio galaxies. In contrast, the fainter and more numerous objects that we appear to be discovering from a combination of deep spectroscopy and archival imaging are more likely to belong to the progenitors of normal present day galaxies. While considerable uncertainties remain, these observations have the potential of giving us rare views of the actual formation of such objects.

ACKNOWLEDGMENTS

We acknowledge helpful discussions with Bob Carswell, Hsiao-Wen Chen, Jeff Cooke, Masami Ouchi and Francois Schweizer. We thank the staff of the Las Campanas Observatory and the Keck Observatory for their help with the observations, and thank Luke Barnes for providing us the results of his simulations. MR is grateful to the IoA in Cambridge and to the Raymond and Beverley Sackler Distinguished Visitor programme for hospitality and support in summer 2011, when some of this work was done. He further acknowledges support from the National Science Foundation through grant AST-1108815. GDB has been supported by the Kavli Foundation. J-RG gratefully acknowledges the financial support of a Millikan Fellowship provided by Caltech.

REFERENCES

Balestra I. et al., 2010, A&A, 512, 12
Barnes L. A., Haehnelt M. G., 2009, MNRAS, 397, 511
Barnes L. A., Haehnelt M. G., 2010, MNRAS, 403, 870
Beckwith S. V. W. et al., 2006, AJ, 132, 1729
Behroozi P. S., Conroy C., Wechsler R. H., 2010, ApJ, 717, 379
Birnboim Y., Dekel A., 2003, MNRAS, 345, 349
Bolton J. S., Haehnelt M. G., 2007, MNRAS, 374, 493
Bouwens R. J. et al., 2010, ApJ, 708, 69
Bridge C. R. et al., 2010, ApJ, 720, 465
Bridge C. R. et al., 2012, preprint (arXiv:1205.4030)
Bunker A. J., Marleau F. R., Graham J. R., 1998, AJ, 116, 2086
Cantalupo S., Lilly S. J., Haehnelt M. G., 2012, MNRAS, 425, 1992
Capak P. et al., 2004, AJ, 127, 180
Cardamone C. N. et al., 2010, ApJS, 189, 270
Cooke J., Berrier J. C., Barton E. J., Bullock J. S., Wolfe A. M., 2010, MNRAS, 403, 1020
da Cunha E., Charlot S., Elbaz D., 2008, MNRAS, 388, 1595
Dekel A., Birnboim Y., 2006, MNRAS, 368, 2
Dekel A. et al., 2009, Nat, 457, 451
Dey A. et al., 2005, ApJ, 629, 654
Dijkstra M., 2009, ApJ, 690, 82
Dijkstra M., Kramer R., 2012, MNRAS, 424, 1672
Dijkstra M., Loeb A., 2009, MNRAS, 400, 1109
Dijkstra M., Haiman Z., Spaans M., 2006, ApJ, 649, 14
Dijkstra M., Lidz A., Wyithe J. S. B., 2007, MNRAS, 377, 1175
Dunlop J. S., McLure R. J., Robertson B. E., Ellis R. S., Stark D. P., Cirasuolo M., de Ravel L., 2012, MNRAS, 420, 901
Fardal M. A., Katz N., Gardner J. P., Hernquist L., Weinberg D. H., Davé R., 2001, ApJ, 562, 605
Faucher-Giguère C.-A., Kereš D., Dijkstra M., Hernquist L., Zaldarriaga M., 2010, ApJ, 725, 633
Finkelstein S. L., Papovich C., Giavalisco M., Reddy N. A., Ferguson H. C., Koekemoer A. M., Dickinson M., 2010, ApJ, 719, 1250
Francis P. J. et al., 1996, ApJ, 457, 490
Fumagalli M., Prochaska J. X., Kasen D., Dekel A., Ceverino D., Primack J. R., 2011a, MNRAS, 418, 1796
Fumagalli M., O'Meara J. M., Prochaska J. X., 2011b, Sci, 334, 1245
Fynbo J. U., Møller P., Warren S. J., 1999, MNRAS, 305, 849
Giavalisco M., and the GOODS Team, 2004, ApJ, 600, L93
Goerdt T., Dekel A., Sternberg A., Ceverino D., Teyssier R., Primack J. R., 2010, MNRAS, 407, 613
Goerdt T., Dekel A., Sternberg A., Gnat O., Ceverino D., 2012, MNRAS 424, 2212
Grazian A. et al., 2006, A&A, 449, 951
Guaita L. et al., 2010, ApJ, 714, 255
Haehnelt M. G., Steinmetz M., Rauch M., 1996, ApJ, 465, 95
Haiman Z., Spaans M., Quataert E., 2000, ApJ, 537, 5
Hansen M., Oh S. P., 2006, MNRAS, 367, 979
Hashimoto T., Ouchi M., Shimasaku K., Ono Y., Nakajima K., Rauch M., Lee J., Okamura S., 2012, preprint (arXiv:1206.2316)
Hayashino T. et al., 2004, AJ, 128, 2073
Hester J. A. et al., 2010, ApJ, 716, 14
Hibbard J. E., Vacca W. D., Yun M. S., 2000, AJ, 119, 1130
Inoue A. K., 2011, MNRAS, 415, 2920
Jimenez R., Haiman Z., 2006, Nat, 440, 501
Kapferer W., Kronberger T., Ferrari C., Riser T., Schindler S., 2008, MNRAS, 389, 1405
Karl S. J., Naab T., Johansson P. H., Kotarba H., Boily C. M., Renaud F., Theis C., 2010, ApJ, 715, 88
Keel W. C., Cohen S. H., Windhorst R. A., Waddington I., 1999, AJ, 118, 2547
Kereš D., Katz N., Weinberg D. H., Davé R., 2005, MNRAS, 363, 2
Kravtsov A. V., Berlind A. A., Wechsler R. H., Klypin A. A., Gottlöber S., Allgood B., Primack J. R., 2004, ApJ, 609, 35
Kudritzki R.-P. et al., 2000, ApJ, 536, 19
Kulas K. R., Shapley A. E., Kollmeier J. A., Zheng Z., Steidel C. C., Hainline K. N., 2012, ApJ, 745, 33
Kunth D., Mas-Hesse J. M., Terlevich E., Terlevich R., Lequeux J., Fall S. M., 1998, A&A, 334, 11
Laursen P., Sommer-Larsen J., Razoumov A. O., 2011, ApJ, 728, 52
Leitherer C., Robert C., Drissen L., 1992, ApJ, 401, 596
Leitherer C. et al., 1999, ApJS, 123, 3
Luo B. et al., 2010, ApJS, 187, 560
Malhotra S., Rhoads J. E., 2002, ApJ, 565, 71
Matsuda Y. et al., 2004, AJ, 128, 569
Matsuda Y. et al., 2011, MNRAS, 410, 13
Matsuda Y. et al., 2012, MNRAS, 425, 878
Mirabel I. F., Dottori H., Lutz D., 1992, A&A, 256, 19
Mori M., Umemura M., Ferrara A., 2004, ApJ, 613, 97
Najarro F., Kudritzki R. P., Cassinelli J. P., Stahl O., Hillier D. J., 1996, A&A, 306, 892
Neufeld D. A., 1991, ApJ, 370, 85
Nilsson K., Fynbo J. P. U., Sommer-Larsen J., Ledoux C., 2006, A&A, 452, L23
Ouchi M. et al., 2009, ApJ, 696, 1164
Palunas P., Teplitz H. I., Francis P. J., Williger G. M., Woodgate B. E., 2004, ApJ, 602, 545
Pettini M., Steidel C. C., Adelberger K. L., Dickinson M., Giavalisco M., 2000, ApJ, 528, 96
Pettini M., Rix S. A., Steidel C. C., Hunt M. P., Shapley A. E., Adelberger K. L., 2002, Ap&SS, 281, 461
Prescott M. K. M., Dey A., Jannuzi B. T., 2009, ApJ, 702, 554
Prescott M. K. M. et al., 2012, ApJ, 752, 86
Quider A. M., Pettini M., Shapley A. E., Steidel C. C., 2009, MNRAS, 398, 1263

Raiter A., Schaerer D., Fosbury R. A. E., 2010, A&A, 523, 64
Rauch M., Haehnelt M. G., 2011, MNRAS, 412, 55
Rauch M., Haehnelt M. G., Steinmetz M., 1997, ApJ, 481, 601
Rauch M. et al., 2008, ApJ, 681, 856
Rauch M., Becker G. D., Haehnelt M. G., Gauthier J.-R., Ravindranath S., Sargent W. L. W., 2011, MNRAS, 418, 1115 (Paper I)
Rosdahl J., Blaizot J., 2012, MNRAS, 423, 344
Roy I., Shu C.-W., Fang L.-Z., 2010, ApJ, 716, 604
Saito T., Shimasaku K., Okamura S., Ouchi M., Akiyama M., Yoshida M., 2006, ApJ, 648, 54
Santos M. R., Ellis R. S., Kneib J.-P., Richard J., Kuijken K., 2004, ApJ, 606, 683
Scarlata M. et al., 2009, ApJ, 706, 1241
Schaerer D., 2002, A&A, 382, 28
Schaerer D., Verhamme A., 2008, A&A, 480, 369
Schaye J., Aguirre A., Kim T.-S., Theuns T., Rauch M., Sargent W. L. W., 2003, ApJ, 596, 768
Schweizer F., 1978, in Berkhuisen E. M., Wielebinski R., eds, IAU Symposium 77, Structure and Properties of Nearby Galaxies. D. Reidel Publ. Co., Dordrecht, p. 279
Shapley A. E., Steidel C. C., Pettini M., Adelberger K. L., Erb D. K., 2006, ApJ, 651, 688
Simcoe R. A., Sargent W. L. W., Rauch M., 2004, ApJ, 606, 92
Smith B. J. et al., 2008, AJ, 135, 2406
Steidel C. C., Adelberger K. L., Shapley A. E., Pettini M., Dickinson M., Giavalisco M., 2000, ApJ, 532, 170
Steidel C. C., Adelberger K. L., Shapley A. E., Pettini M., Dickinson M., Giavalisco M., 2003, ApJ, 592, 728
Steidel C. C., Bogosavljevic M., Shapley A. E., Kollmeier J. A., Reddy N. A., Erb D. K., Pettini M., 2011, ApJ, 736, 160
Taniguchi Y., Shioya Y., 2000, ApJ, 532, L13
Tapken C., Appenzeller I., Noll S., Richling S., Heidt J., Meinköhn E., Mehlert D., 2007, A&A, 467, 63
Tenorio-Tagle G., Silich S. A., Kunth D., Terlevich E., Terlevich R., 1999, MNRAS, 309, 332
Tonnesen S., Bryan G. L., 2010, ApJ, 709, 1203
Tonnesen S., Bryan G. L., 2012, MNRAS, 422, 1609
Tumlinson J., Shull J. M., 2000, ApJ, 528, 65
Tumlinson J., Shull J. M., Venkatesan A., 2003, ApJ, 584, 608
van de Voort F., Schaye J., Booth C. M., Haas M. R., Dalla Vecchia C., 2011, MNRAS, 414, 2458
Venemans B. P. et al., 2005, A&A, 431, 793
Verhamme A., Schaerer D., Maselli A., 2006, A&A, 460, 397
Verhamme A., Schaerer D., Atek H., Tapken C., 2008, A&A, 491, 89
White S. D. M., Rees M. J., 1978, MNRAS, 183, 341
Whitmore B. C., Schweizer F., 1995, AJ, 109, 96
Wolf C., Dye S., Kleinheinrich M., Meisenkaiser K., Rix H.-W., Wisotzki L., 2001, A&A, 377, 442
Xu W., Wu X.-P., Fang L.-Z., 2011, MNRAS, 418, 853
Yamada T., Matsuda Y., Kousai K., Hayashino T., Morimoto N., Umemura M., 2012, ApJ, 751, 29
Yang Y., Zabludoff A., Tremonti C., Eisenstein D., Davé R., 2009, ApJ, 693, 1579
Yang Y., Zabludoff A., Eisenstein D., Davé R., 2010, ApJ, 719, 1654
Yang Y., Zabludoff A., Jahnke K., Eisenstein D., Davé R., Shectman S. A. Kelson D. D., 2011, ApJ, 735, 87
Yoshida M. et al., 2008, ApJ, 688, 918
Yoshida M., Yagi M., Komiyama Y., Furusawa H., Kashikawa N., Hattori T., Okamura S., 2012, ApJ, 749, 43

APPENDIX A: THE EFFECT OF A FINITE RECOMBINATION TIME-SCALE ON THE OBSERVED L*yα* FLUX AND EQUIVALENT WIDTH

After the injection of ionizing photons by a short starburst into the surrounding interstellar and intergalactic gas the ionized gas recombines, accompanied by the emission of a proportional fraction of Lyα photons. The recombination process will delay and drag out the emission of Lyα photons, relative to the production rate of the ionizing photons and the stellar continuum. Assuming that the gas is near the virial overdensity ($1 + \delta \sim 180$ for a recently collapsed halo at $z = 2.63$), the recombination time-scale is

$$\tau_{\rm rec} = (N_{\rm e}\alpha_{\rm rec})^{-1} \sim 5.4 \times 10^7 \ {\rm yr} \left(\frac{1+\delta}{180}\right). \quad \text{(A1)}$$

As the time-scales for the escape of Lyα photons through scattering even from an optically thick halo are usually shorter than that (Roy, Shu & Fang 2010; Xu, Wu & Fang 2011), recombination will dominate the evolution of the emergent Lyα flux. The delayed release of the Lyα photons will render the emitter visible for a longer time and may explain how a wave of instantaneous star formation passing through a filament (e.g. in a turbulent wake) can maintain similar flux levels along the filament, even though the starburst may be of much shorter duration than the time it takes for the filament to extend to its current length. The time evolution of the equivalent width of Lyα (the ratio between Lyα line flux and continuum flux density) is dependent on both the changes of the (retarded) line flux and the more quickly decaying continuum flux. If the broad-band continuum flux fades more rapidly than the recombinations can occur, the observed equivalent width can rise and stay high for a significant amount of time. Fig. A1 shows the predicted rest-frame equivalent width versus time after a starburst, for a $z = 2.63$ instantaneous starburst with $7 \times 10^7\,{\rm M}_\odot$ in stars, a metallicity of $Z = 0.0004$ and otherwise default assumptions, simulated with the STARBURST99 code. The time evolution of the Lyα flux was simply convolved with an exponential kernel with width $\tau_{\rm rec}$. Even though the *B*-band continuum luminosity drops by a factor of 23 over the first 5×10^7 yr, the Lyα flux drops less rapidly, so the equivalent width stays high or remains rising for all but the shortest one of the time-scales

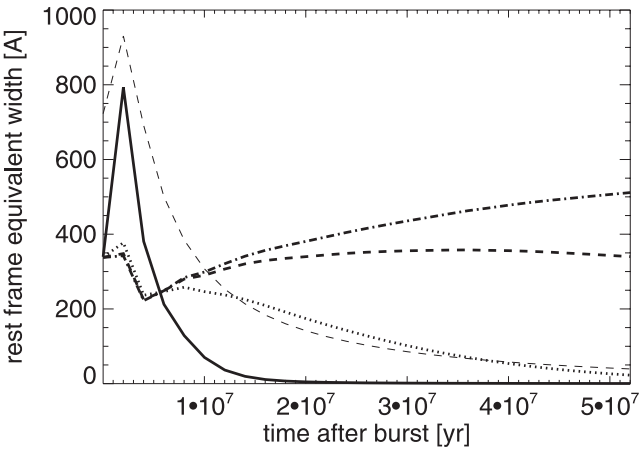

Figure A1. The predicted rest-frame equivalent width versus time after a starburst, for a $z = 2.63$ instantaneous starburst with $7 \times 10^7\,{\rm M}_\odot$ in stars, with a metallicity of $Z = 0.0004$. The models here assume instantaneous ionization, but recombination (and emission of Lyα) with a recombination time-scale $\tau_{\rm rec}$. The thick solid, dotted, dashed and dash–dotted graphs are for $\tau_{\rm rec} = 10^6$, 10^7, 5.4×10^7 and 5×10^8 yr, respectively. Because of the delayed emission of Lyα photons, the equivalent width rises to considerable values, while the flux in the *B* band drops by a factor of 23 over the first 5×10^7 yr. The rapid variation during the first 10^7 yr is caused by the delayed rise of the stellar (*B* band) continuum luminosity relative to the production rate of ionizing photons. In addition to the equivalent widths, the plot also shows the evolution of the Lyα line flux for the $\tau_{\rm rec} = 5.4 \times 10^7$ yr case, as the thin dashed line, in arbitrary units.

shown. While the instantaneous equivalent width would be as high as 800 Å, the recombination delay would make this stage unobservable, and the rapid decay would render finding a galaxy in this state quite rare. The plot shows the effect of different densities, with the dashed line marking the recombination time for an overdensity of 180 at $z = 2.63$, and the longer (shorter) time-scales corresponding to lower (higher) gas densities. The effect may explain how Lyα radiation, after a starburst, may remain visible longer than the stellar continuum light. It may also account for some of the observations of unusually large equivalent widths of Lyα emitters (e.g. Malhotra & Rhoads 2002), without having to invoke exotic stellar populations or the peculiar propagation of Lyα photons in the presence of a clumpy and dusty medium (e.g. Neufeld 1991; Hansen & Oh 2006).

APPENDIX B: CONSTRAINTS FROM SURFACE BRIGHTNESS PROFILES ON THE EMISSION MECHANISM OF Lyα EMITTERS

Most Lyα emitters, regardless of luminosity or how they are detected, and for the entire range of luminosities observed, have singly peaked, somewhat extended surface brightness profiles (e.g. Rauch et al. 2008). In the spectral direction they show the well-known double-humped emission profiles with a dominant red peak, showing a broad shoulder to the red and a sharp drop in the blue (e.g. Tapken et al. 2007; Rauch et al. 2008; Kulas et al. 2012; Yamada et al. 2012). A hint of the blue peak can often be discerned (see e.g. fig. 3 of Rauch et al. 2008), but at greatly reduced flux levels compared to the red peak. Profiles where the blue peak dominates over the red one are rare, and are generally thought to signify infalling gas (see e.g. Rauch et al. 2008, fig. 18).

The fluxes and likely masses of the typical Lyα emitters and their spatial compactness suggest that they are consistent with being powered by stellar ionization from a single internal source, at least in the innermost 10–20 kpc. However, because of a lack of deep two-dimensional spectroscopy this assumption has not been directly tested so far, and direct comparisons between individual observed and simulated surface brightness profiles have not been performed.

Simplified, spherically symmetric models have explored several possible basic scenarios for the formation of the Lyα emission line. The models examined fall under the basic categories of outflows and infall of gas. Among the outflow models, the emission of Lyα from wind shells (e.g. Pettini et al. 2000, 2002; Verhamme, Schaerer & Maselli 2006; Schaerer & Verhamme 2008; Verhamme et al. 2008; Quider et al. 2009) has received the most attention. These models are capable of giving quite realistic representations of the one-dimensional spectra of Lyα break galaxies (e.g. Verhamme et al. 2006, 2008; Tapken et al. 2007). However, Barnes & Haehnelt (2010) have pointed out that shells generally lead to a shallow surface brightness profile, which may be different from what is observed in actual two-dimensional observations of Lyα emitters (e.g. Rauch et al. 2008). Collapsing protogalactic haloes have been modelled by Dijkstra, Haiman & Spaans 2006; Barnes & Haehnelt 2009, 2010). These models do produce peaked emission with extended low surface brightness aprons, but, at least in the absence of intergalactic absorption, they do not get the correct preponderance of the red peak over the weaker (or absent blue peak). However, as the spectral features of those spherically symmetric models are reversible under a sign change of the velocity profile, these models can also be used to represent outflowing motion.

Because of the considerable depth of our spectra (Fig. 5), we can test the various hypotheses about the origin of Lyα directly on individual galaxies without having to resort to stacks.

Fig. B1 again shows the Lyα emission profiles from Fig. 6, now with several different slit profiles from models by Barnes & Haehnelt (2010) overplotted. The models are fits only in so far as the overall flux has been normalized – i.e. they all have the same area under the curves, and their spatial position along the slit has been slightly adjusted by hand to account for the fact that the observed Lyα profiles are not quite lining up with the origin defined by the continuum traces. The Barnes & Haehnelt inflow models introduced by Dijkstra et al. (2006) are parametrized by a power-law dependence of the radial velocity on the radius, i.e. $v \propto -r^{\alpha}$, with power-law indices $\alpha = -0.5$ for accelerated infall of massless shells and $\alpha = 1.0$ for spherical top-hat collapse. As pointed out above, only a few emitters show dominant blue components of the double-humped profile (Rauch et al. 2008; Kulas et al. 2012; Yamada et al. 2012). There are several explanations for this, the relative importance of which is not yet fully understood. Intergalactic absorption would erode blue peaks (Dijkstra, Lidz & Wyithe 2007; Laursen, Sommer-Larsen & Razoumov 2011), as would an outflow of gas away from the stellar source of ionizing photons (e.g. Kunth et al. 1998; Tenorio-Tagle et al. 1999; Verhamme et al. 2006). In the case of a generic outflow scenario, reversing the velocity vector will flip the dominant blue peak from the infall picture into a dominant red one, but the surface brightness and column density profiles remain unchanged. We can thus use the Barnes & Haehnelt models to study outflow situations as well, keeping in mind that the $\alpha = -0.5$ surface brightness profiles now correspond to a decelerating outflow (or decelerating expanding halo), and the $\alpha = 1.0$ case becomes an accelerating outflow (expansion). The resulting profiles as seen through the spectrograph slit and collapsed perpendicular to the slit like the real data are shown in Fig. B1. The profiles have been smoothed with an FWHM = 0.9 arcsec wide kernel to account for the finite observed size of the stellar continuum (1.0 and 0.9 arcsec for the two galaxy continua just redward of Lyα emission line).

The two smooth solid lines show the $\alpha = -0.5$ models (decelerated outflow) for total halo masses 10^{11} and $10^{12}\,\mathrm{M}_{\odot}$. After the global scaling with flux, the lower mass halo seems to have a surface brightness profile too concentrated to match the observed profile within the central few arcseconds that we can address here. Better agreement (although still with slightly too narrow wings) is obtained from the $10^{12}\,\mathrm{M}_{\odot}$ model. The dotted lines are for the $\alpha = 1$ (accelerated outflow) models with the same halo masses of 10^{11} and $10^{12}\,\mathrm{M}_{\odot}$ (the wider profile is from the higher mass halo). For those (accelerating) models, the lower mass one (thin dotted line) gives a fit approximately as good as the decelerating, $\alpha = -0.5$, higher mass case, but now overestimating the width of the observed surface brightness profiles somewhat. The dashed line is the $N(\mathrm{H\,I}) = 2 \times 10^{22}\ \mathrm{cm}^{-2}$ wind shell of fig. 6 of Barnes & Haehnelt (2010).

For $\alpha = -0.5$ with their very strongly peaked narrow profiles, the agreement with the observation is obviously sensitive to the degree of smoothing involved. We found that a slightly larger Gaussian smoothing window (1.5 arcsec instead of the 1 arcsec FWHM) gives almost perfect agreement with the observed profile, but we did not see such a smoothing physically warranted to implement it. In reality, however, the source of ionizing photons would be a galaxy subject to patchy emission and peculiar motions which soften the very sharp emission peak that characterizes the *decelerated* models. Given the number of additional degrees of freedom, including the column density, concentration parameter and the possibility of other, more physically motivated velocity–radius relations, the

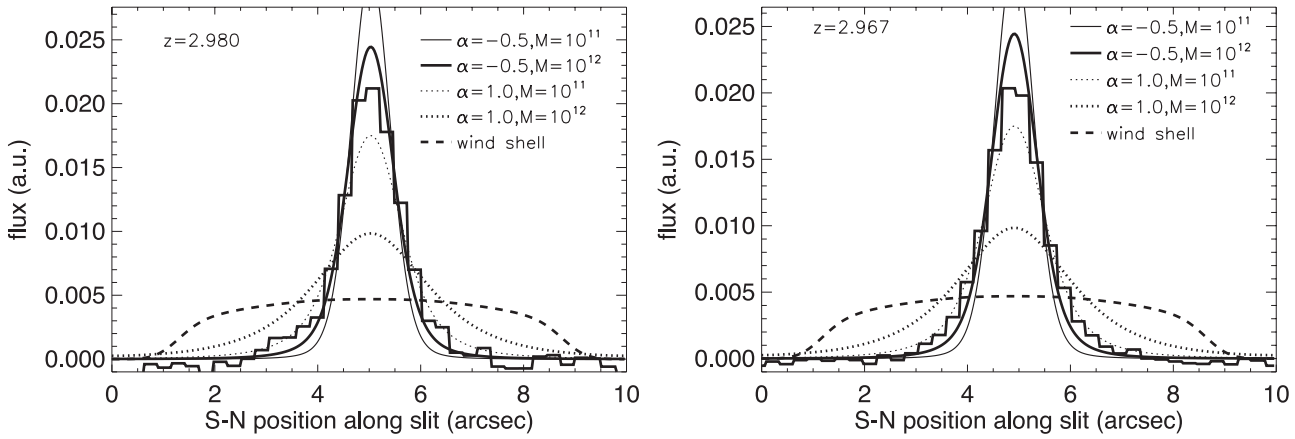

Figure B1. The same two spatial Lyα profiles along the slit as in Fig. 6 (solid histogram), but now overplotting the predicted profiles expected from the surface brightness distributions of various models by Barnes & Haehnelt (2010). These models assume gaseous haloes in different kinematic stages, surrounding a point source of ionizing radiation. The thin and thick solid lines show the $\alpha = -0.5$ models for total halo masses 10^{11} and $10^{12}\,M_{\odot}$, respectively. For the observed red-dominant peaks this model corresponds to a decelerated outflow. The thin and thick dotted lines are for the $\alpha = 1$ models with halo masses 10^{11} and $10^{12}\,M_{\odot}$ (the wider profile is from the higher mass halo) and correspond to accelerating outflows. The dashed line is the $N(\mathrm{H\,I}) = 2 \times 10^{22}$ cm^{-2} wind shell of fig. 6 of Barnes & Haehnelt (2010). The profiles have been smoothed with an FWHM = 0.9 arcsec wide kernel.

current snapshot of model parameters cannot be expect to deliver any strong constraints on the nature of the velocity field. The relatively concentrated spatial surface brightness profiles suggest, however, that the overall velocity gradients involved in the formation of the Lyα line do not exceed a couple of hundred km s^{-1}, which is also indicated by the small velocity offsets observed between the Lyα emission line and the systemic velocity for bright, compact Lyα emitters (e.g. Hashimoto et al. 2012). Large velocity gradients of up to 800 km s^{-1} as seen in low ionization absorption troughs of Lyman break galaxies (Steidel et al. 2011) do not seem to contribute noticeably to the Lyα emission line formation (see also Dijkstra & Hultman Kramer 2012). The wind-shell model, at least in its implementation as a large-scale shell with large covering factor, while producing a realistic one-dimensional spectral line profile, appears inconsistent with the observations on account of its overly extended predicted surface brightness profile.

We conclude that, irrespective of the precise velocity field, the inner ∼20 kpc of the emission surface profiles of strong Lyα emitting galaxies can be modelled by point sources of ionizing radiation embedded in slowly expanding, optically thick gaseous haloes.

This paper has been typeset from a TEX/LATEX file prepared by the author.